Nanoscale

PAPER

View Article Online
View Journal | View Issue

Cite this: *Nanoscale*, 2018, **10**, 22963

Super-alkalis as building blocks of one-dimensional hierarchical electrides†

Hong Fang, *‡[a] Jian Zhou‡[b] and Puru Jena*[a]

Received 18th September 2018,
Accepted 23rd November 2018

DOI: 10.1039/c8nr07609j

rsc.li/nanoscale

Electrides are ionic compounds where localized electrons act as anions. Because of their exotic properties in optoelectronics and catalysis, electrides have attracted considerable interest in recent years and many electrides, with anionic electrons distributed in zero-, one-, two- and three-dimensions, have been studied. Here, using first-principles calculations, we report a different class of inorganic electrides where Li_3O super-alkali clusters form the building blocks of one-dimensional hierarchical structures, characterized by the presence of localized electrons with high charge density along a one-dimensional chain. We further show that the stability of this electride can be improved by embedding it inside a BN nanotube (BNNT). In addition, Li_3O@BNNT exhibits powerful reducing ability as well as anti-ferromagnetism, highlighting the importance of nano-assembly in the development of new stable electrides with novel properties.

Introduction

Electrides, named by Dye *et al.* four decades ago,[1] constitute an interesting family of ionic compounds whose anion components are not atoms, but electrons localized in cavities of the structures. These anionic electrons are reminiscent of color centers in alkali-halide crystals. However, instead of being localized at defect sites, anionic electrons in electrides are arranged in a periodic lattice. These non-nucleus-bound electrons exhibit high mobility and low work function, which enable applications of electrides as high-performance optoelectronic devices[2,3] and catalytic agents.[4–7] Ever since the first discovery of room-temperature stable electride $(Ca_{24}Al_{28}O_{64})^{4+}\cdot 4e^-$,[8,9] many more electrides, characterized by their zero-, one-, two-, and three-dimensionally distributed anionic electrons, have been synthesized experimentally and predicted theoretically using first-principles methods.[10–17] Efforts are under way to identify and categorize these newly found electrides as well as study their electronic and magnetic properties.[10–20]

In this paper, using first-principles computational methods, we report a different class of inorganic electrides where super-alkalis are the building blocks. Super-alkalis are clusters of atoms that mimic the chemistry of alkali atoms, but the energy to remove an electron from a super-alkali is significantly less than the ionization energy of any alkali atom. First proposed in 1984 by Gutsev and Boldyrev,[21] super-alkalis consisted of clusters, M_xA, where the number (x) of alkali metal atoms M surpass the valence of the anion A by one. This cluster has one "redundant" electron, contributed by the outnumbered alkali metal atom, which it can readily lose to become a cluster-cation $(M_xA)^+$. The main characteristic of electrides is that, once the electron is detached, it should remain localized, forming a periodic pattern. We hypothesized that, because an electron can be easily detached from a super-alkali, loosely bound electrons in the super-alkalis could serve as anionic electrons of an electride, if such electrons remain localized in a periodic pattern. Considerable research over the past decade has identified numerous super-alkalis by using electron-counting rules, known in chemistry for over a century.[22] Thus, if super-alkalis could be used as building blocks, it could vastly increase the pool of electrides.

To prove the above hypothesis, we chose Li_3O, a well-known super-alkali. In the gas phase, Li_3O cluster adopts a planar configuration (see Fig. S1a in ESI†) and has an ionization potential (IP) of 3.88 eV, which is much smaller than that of the Li atom (5.62 eV). Due to the attraction between the lone pair of the oxygen and the positive charge on the Li cations, Li_3O clusters interact with each other strongly.[23] We show that, under certain constrained environment, these clusters self-assemble to a chain structure (see Fig. S1b of ESI†). We carried out a computational study of the properties of one-dimensional nano-structures assembled from Li_3O super-alkali clus-

[a]*Department of Physics, Virginia Commonwealth University, Richmond, VA 23284, USA. E-mail: pjena@vcu.edu, hfangtom@gmail.com*
[b]*Center for Advancing Materials Performance from the Nanoscale, State Key Laboratory for Mechanical Behavior of Materials, Xi'an Jiaotong University, Xi'an, 710049, China*

†Electronic supplementary information (ESI) available. See DOI: 10.1039/c8nr07609j

‡These are co-first authors.

ters and show that Li_3O can be polymerized to be one-dimensional electride $Li_3O^+ \cdot e^-$. The resulting material is dynamically and thermally stable. Further, we explored its magnetic and catalytic properties originating from the anionic electrons, finding it to be anti-ferromagnetic and a powerful reducing agent.

Stability of one-dimensional (1D) Li_3O chain

As pointed out before, the geometry of Li_3O cluster is planar. However, when two Li_3O clusters come close to each other, the lone pair on the oxygen of one Li_3O cluster attract (repulse) the lithium (oxygen) of the other Li_3O, making a pyramidal configuration, with oxygen out of the (Li_3) plane (see Fig. S1a†). As more Li_3O units come together, a stable chain structure forms with oxygen linking the Li_3 planes. According to this "growth" model, a periodic chain, with the unit cell given in Fig. 2a, is expected. We optimized the geometry of $(Li_3O)_n$ clusters as a function of n, which eventually leads to an infinite chain as n approaches ∞. As shown in Fig. 2b, there are no imaginary modes in the calculated phonon spectrum; hence the chain is lattice dynamically stable. The calculated electronic structure, given in Fig. 2c, shows that the Li_3O chain is metallic. The flattened bands in both phonon and electronic structures, especially the dispersion-less feature along the X–M direction, are results of quantum confinement, originating from the one dimensionality of the material.

We investigated the thermal stability of the 1D Li_3O using molecular dynamics simulations at room temperature (300 K) and found the structure to be stable, as shown in Fig. S2a of ESI.† We further drew the Li–O phase diagram using data from the Materials Project.[24] Assuming that the three-dimensional (3D) Li_3O adopts the same crystal structure of Cs_3O,[16] where 1D Li_3O chains are aligned in a hexagonal lattice (Fig. S3 of ESI†), the calculated energetics indicate that Li_3O lies above the convex hull (Fig. S4 of ESI†). This suggests that Li_3O is metastable against stable oxide Li_2O.

Li_3O as an electride

To see if the 1D Li_3O is an electride, we first studied the electron localization function (ELF) of the system. ELF measures the degree of electron localization and has a value from 0 to 1. ELF = 0.5 corresponds to free electron gas, while ELF = 1 corresponds to fully localized electrons with the same charge density. For light elements with s and p electrons, localized electrons exhibit ELF values around or above 0.7. For heavy elements with d and f electrons, ELF shows a value around 0.2–0.3. As shown in Fig. 3a, for the 1D Li_3O, localized electrons with ELF $\geq$ 0.7 (colored in yellow) form shells outside each Li_3 plane around the chain structure. The calculated charge density, integrated along the chain axis and given in Fig. 3b, shows periodic peaks corresponding to the positions of these localized electrons. The coexistence of high charge density and localized electrons provide the signature of anionic electrons in an electride.[12,17] The appearance of localized valence electrons around the outside of the Li_3O chain is similar to the case of dicalcium nitride which has layers of anionic electrons residing in the outside of atomic layers.[25] The material is identified as an electride signaled by high charge density concurred with large ELF values around 0.7.[25]

As an electride, the 1D Li_3O is expected to have low work function for the anionic electrons. By gradually increasing the number of $Li_3O^+ \cdot e^-$ units, as demonstrated in Fig. 1, the ratio between the number of lithium and the number of oxygen atoms in the structure can be increased. Meanwhile, the system will act more and more like an alkali metal with ever-decreasing IP and energy gap. The extrapolated end-point at ratio N_{Li}/N_O = 3 corresponds to the periodic 1D Li_3O, which has a zero band gap. The extrapolated IP of the 1D material is 3.0 eV, which is consistent with the calculated work function (Fig. S5 of ESI†) of 2.5 eV. Such value is similar to the lowest work function of 2.6 eV measured in dicalcium nitride – a material once considered as having the most delocalized anionic electronic system in the electride family.[25] This suggests that the anionic electrons of the 1D Li_3O are highly delocalized from the chain of atoms. The electride, therefore, can serve as a powerful reducing or catalytic agent. However, the ultra-low work function and the metallicity of the 1D Li_3O also means that it could be very reactive. This will limit the potential applications of the 1D Li_3O electride. For instance, if the electride is used in gas conversion, instead of serving as a catalyst to reduce the gas, the chain structure could likely be destroyed by reaction with the gas molecules.

One-dimensional hierarchical structure

We studied ways to improve the stability of 1D Li_3O, without adversely affecting its reducing power. To this end, we embedded the 1D Li_3O inside a (4,8) boron-nitride nano-tube

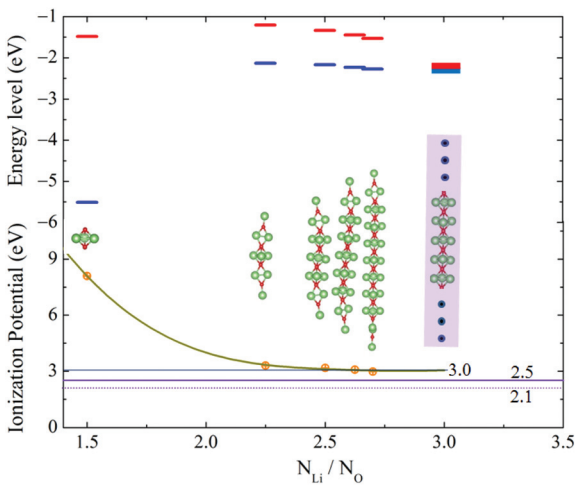

Fig. 1 Calculated energy gap and IP for chain structures with increasing ratio between the numbers of lithium atoms (N_{Li}) *vs.* the number of oxygen (N_O) in the compositions. The red and blue bars represent the LUMO and HOMO, respectively. The extrapolated point at N_{Li}/N_O = 3 corresponds to the 1D Li_3O electride. With elevated lithium composition, both the energy gap and the IP of the structure decrease. The solid line in purple shows the value of calculated work function of the 1D Li_3O and the dotted line shows the calculated work function of Li_3O@BNNT.

(BNNT). Because the BNNT is a wide-gap semiconductor, it will not react with the gas molecules, while allowing 1D Li_3O to contribute its electrons due to the very low work function. In addition, because BNNT is hydrophobic, H_2O molecules which are often present during the gas conversion process, would not adversely affect the reaction. According to our calculations, 1D Li_3O@BNNT leads to a highly preferred exothermic reaction, releasing 0.66 eV per oxygen. The diameter of the tube is chosen to prevent bond formation between the Li_3O and the BNNT. Fig. 4 shows the optimized structure of Li_3O@BNNT and its calculated electronic (partial) density of states (DoS). Although pure BNNT is a wide-gap semiconductor, the combined material becomes metallic. The energy gap between −4 to −1 eV corresponds well with the gap present within the pure Li_3O chain in Fig. 2c.

Interestingly, Li_3O@BNNT remains an electride. This is evident from the concurrence of the positive difference charge density and the large ELF value on the Li_3 plane. The difference charge density is computed by subtracting the charge densities of BNNT and Li_3O from that of Li_3O@BNNT. For this calculation, the structures of BNNT and Li_3O in Li_3O@BNNT are maintained, while only their electrons are allowed to redistribute. As shown in Fig. 5, the anionic electrons, signaled by large charge density and large ELF, reside lopsidedly in the vacant space between the Li_3O chain and BNNT. The calculated work function of Li_3O@BNNT is only 2.1 eV, even lower than the 2.5 eV of the 1D Li_3O. Thus, Li_3O@BNNT is a hier-

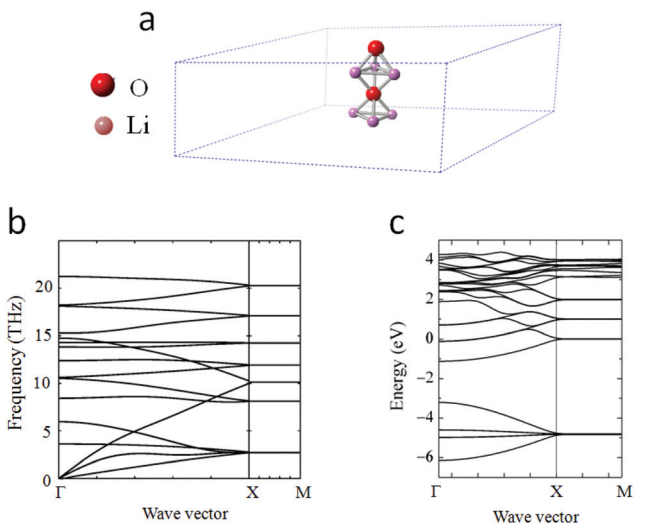

Fig. 2 (a) Optimized unit cell of 1D Li_3O. (b) Calculated phonon spectrum of the material. (c) Calculated electronic band structure of the material with the Fermi level at 0 eV.

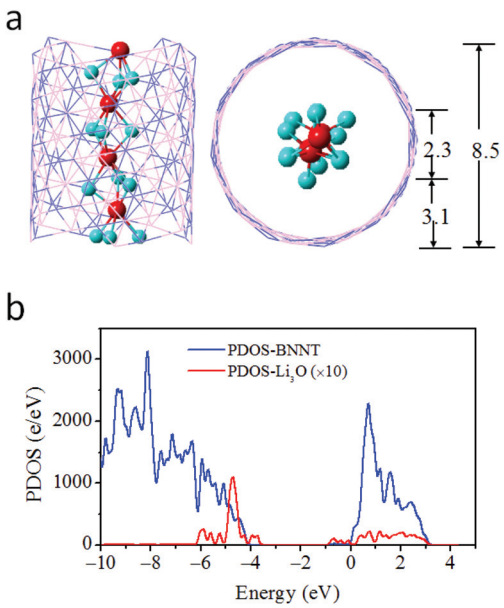

Fig. 4 (a) Optimized unit cell of Li_3O@BNNT. Dimensions of the structure are in Å. (b) Calculated (partial) electronic density of states of Li_3O@BNNT. The Fermi level is at 0 eV. Oxygen atoms are in red and lithium in cyan.

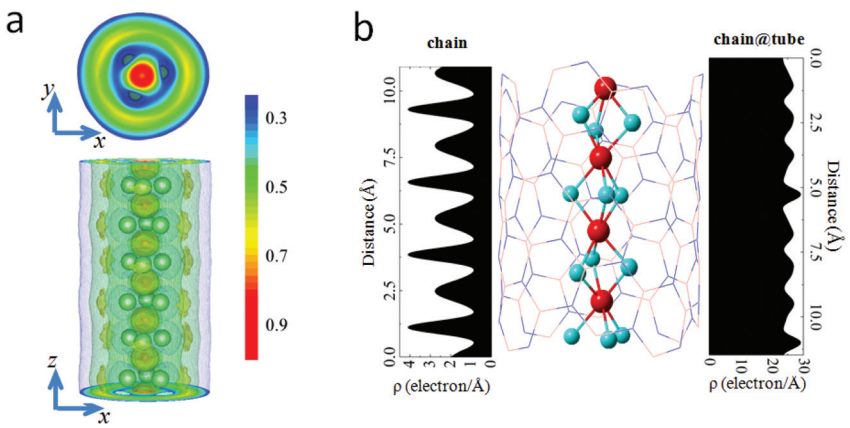

Fig. 3 (a) Calculated electron localization function (ELF) of the 1D Li_3O. The localized electrons with ELF ≥ 0.7 are found as shells around the chain on the (Li_3) planes. (b) Calculated charge density integrated along the chain axis for both the 1D Li_3O and Li_3O@BNNT. Peaks are present at the positions of the localized electrons. Oxygen atoms are in red and lithium in cyan.

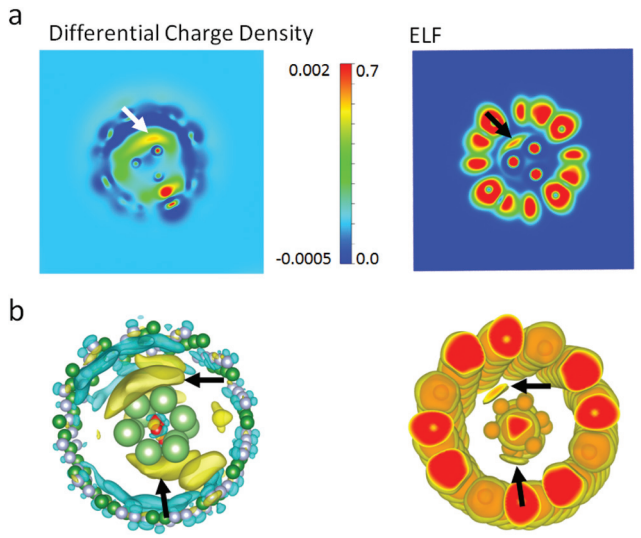

Fig. 5 (a) Left panel: Calculated difference charge density on one Li_3 plane, defined as $C_{Li_3O@BNNT}-C_{BNNT}-C_{Li_3O}$. The unit is "electrons per $Bohr^3$". Right panel: ELF calculated at Li_3 plane for Li_3O@BNNT. The arrows in both panels indicate the concurrence of positive difference charge density and large ELF between the chain and the tube – a signature for the presence of anionic electrons. (b) Corresponding difference charge density (isosurfaces >0.001 electrons per $Bohr^3$ highlighted) and ELF (isosurfaces >0.5 highlighted) displayed in 3D style to show the positions (indicated by the arrows) of the anionic electrons relative to the atoms.

archical electride, with enhanced stability and reduced power. Interestingly, it has been found that inorganic electrides can be formed by adding alkali metals to pure silica zeolites, in which case anionic electrons appear in vacant space along the metal chains residing in the channels of the zeolite.[26] An analogy can be drawn here with Li_3O@BNNT, where a "super-alkali metal", Li_3O, is adding to the channel of BNNT, forming a new inorganic electride.

CO_2 activation using Li_3O@BNNT

The ultra-low work function of the hierarchical electride would make it easy to transfer electrons to carbon dioxide (CO_2) molecule and hence could activate it by bending its linear ground state structure, as is the case with CO_2^-. Note that the activation of CO_2 to CO_2^- is a key step towards converting this gas.[27] The C–O–C angle of CO_2^- is 137° and its stretched C–O bond is 1.24 Å, compared to the 1.15 Å of its neutral ground state.[27] As shown in Fig. 6a, the unit cell of Li_3O@BNNT can readily activate a CO_2 molecule to a bent configuration, with an O–C–O angle of 129° and stretched C–O bond of 1.28 Å. About 1.3 electrons (0.32 per Li_3O in average) are transferred from Li_3O@BNNT to CO_2. The binding energy between Li_3O@BNNT and the CO_2 molecule is 1.1 eV. All these results suggest that the electride can efficiently capture and activate CO_2. In fact, more than one CO_2 molecules can be simultaneously activated, as demonstrated in Fig. S6,† where the four activated CO_2 molecules have an average O–C–O angle of 146°. We note that, without the Li_3O chain inside, the empty BNNT cannot adsorb and activate CO_2. Further calculations

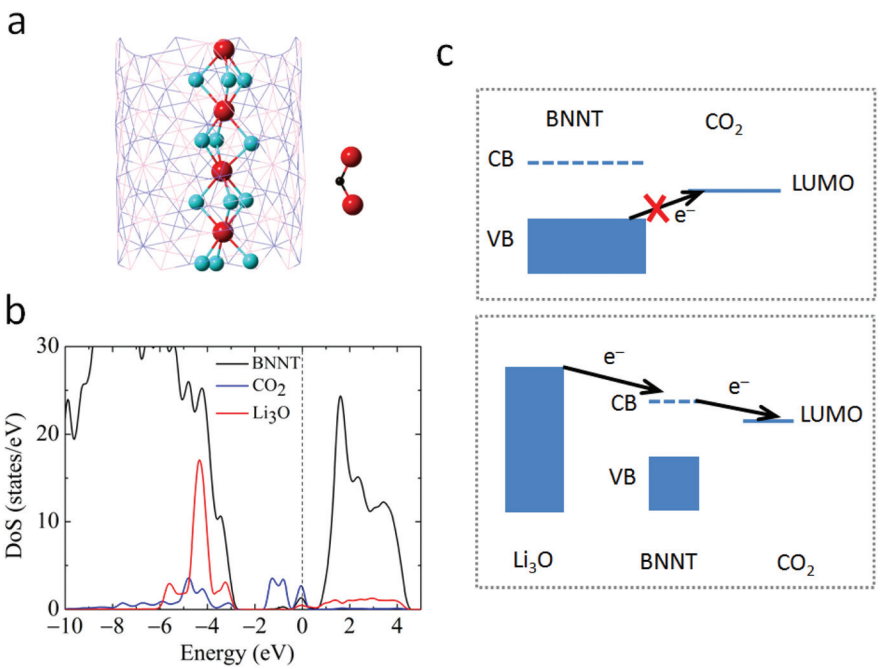

Fig. 6 (a) Optimized structure of Li_3O@BNNT with an adsorbed CO_2 molecule. Oxygen is in red, lithium in cyan and carbon in black. (b) Calculated (partial) electronic density of states (DoS), showing the band alignment between Li_3O, BNNT and CO_2. (c) Schematics of a band model to explain the electron transfer from Li_3O to CO_2 molecule. The upper panel corresponds to case without Li_3O, while the lower panel refers to the case after Li_3O insertion.

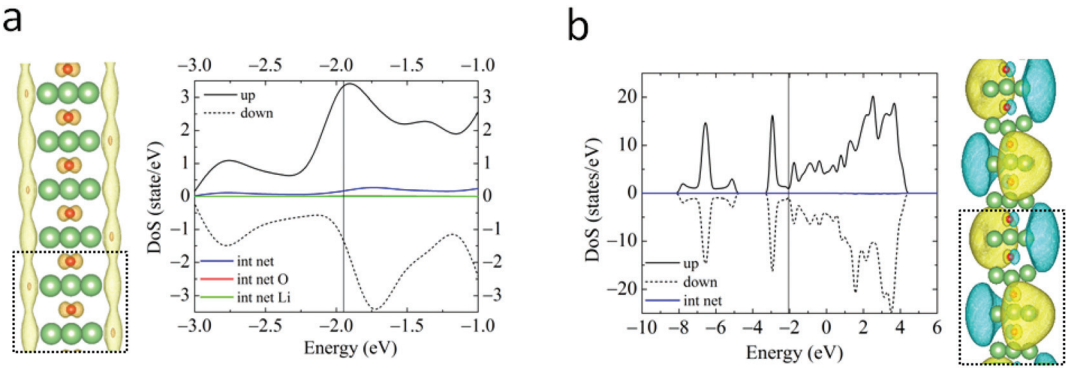

Fig. 7 (a) Calculated spin density and electronic DoS of the ferromagnetic state of Li_3O using the unit cell containing two $Li_3O^+ \cdot e^-$ units. (b) Calculated spin-charge density and electronic DoS of the anti-ferromagnetic state of Li_3O using the unit cell containing four $Li_3O^+ \cdot e^-$ units. The net spins are contributed by the anionic electrons in the structure.

reveal that other small molecules, such as H_2 and H_2O, do not interact with the BNNT; thus, the Li_3O chain is protected.

To understand the activation process, we calculated the (partial) electronic DoS of Li_3O@BNNT·CO_2, as shown in Fig. 6b. According to the Bader charge analysis on the unit cell in Fig. 6a, Li_3O loses 2.71 electrons in total, 1.44 of which is taken by BNNT and the rest 1.27 is taken by the CO_2 molecule. Based on these results, a band model can be used to explain the process. Without the inserted Li_3O, as shown in the upper panel of Fig. 6c, the LUMO of CO_2 molecule is above the valence band (VB) of BNNT, preventing the electron transfer from the tube to the molecule. After the insertion of Li_3O, the Fermi level of the metallic chain is above the conduction band (CB) of BNNT and the tube will be readily n-doped. Now with electrons in the conduction band above the LUMO of CO_2, electrons are easy to transfer to the molecule. These are shown in the lower panel of Fig. 6c. Given that the Li_3O chain at the core of the hierarchical structure is metallic, it is possible to replenish the transferred electrons by keeping the chain in contact with an electron reservoir.

Magnetic property of the electride

Another interesting property of anionic electrons in electrides is their contribution to magnetism. Studies, thus far, have focused on organic electrides[19,20] and electrides with heavy transition metals.[14,18] However, very few reports are available for inorganic electrides, composed of light elements. We, therefore, studied the magnetic states of the 1D Li_3O. With the unit cell containing two $Li_3O^+ \cdot e^-$ units, the electride has a ferromagnetic ground state, which is 17 meV/Li_3O lower in energy than that of the nonmagnetic state. The calculated spin charge density reveals that the net spins coincide with the position of the anionic electrons around the (Li_3) plane, as shown in Fig. 7a. The calculated electronic DoS confirms that the anionic electrons contribute to the net spins, since the spin density from either lithium or oxygen is zero at the Fermi level (Fig. 7a). The magnetic moment on the anionic electrons is found to be 0.21μ_B/Li_3O. However, if the unit cell is doubled with four $Li_3O^+ \cdot e^-$ units, the ground state becomes anti-ferromagnetic. This anti-ferromagnetic state is 45 meV/Li_3O lower than that of the ferromagnetic state. The corresponding spin-density and the electronic density of states are shown in Fig. 7b. The anionic electrons of every two $Li_3O^+ \cdot e^-$ units group into opposite spins, which is consistent with the localized nature of paired electrons. Because of the Coulomb repulsion, the different pairs of electrons partition the space along the chain into different localized regions (Fig. 7b). The behavior is similar to that of the recently reported Mott-insulating electrides α- and β-Yb_5Sb_3, where the anionic electrons, instead of metal elements, serve as the localized magnetic centers with large moments.[28] Although the anionic electrons seem to be much more localized given the strong correlation in these systems, an alternatively up-and-down spin distribution along one dimension is also observed[28] as that in $Li_3O^+ \cdot e^-$. It turns out that the 1D Li_3O is an ideal system to demonstrate the anti-ferromagnetic behavior, consistently found in electrides.[19,20]

Conclusion

In this work, we show that super-alkalis, known in cluster science for decades, can be used as building blocks of inorganic electrides, consisting of light elements. Using Li_3O super-alkali as an example, we found that it could form an electride with one-dimensional structure. Embedding this one-dimensional chain inside a boron-nitride nanotube (BNNT) produces an electride with 1D hierarchical structure and improved stability and properties. For example, Li_3O@BNNT possesses ultra-low work function, making it an ideal material capable of activating CO_2. In addition, Li_3O electride is anti-ferromagnetic, with the anionic electrons carrying the magnetic moment. We note that, recent studies based on data mining of crystalline materials have revealed bulk Cs_3O and Li_4N to be electrides.[16,17] The cluster counterparts of these materials are super-alkalis. In Cs_3O cluster, the valence of oxygen ($V_O = 2$) is less than $3 \times V_{Cs}$ by one, where $V_{Cs} = 1$ is the valence of Cs. Similarly, in Li_4N, the valence of N is 3 which is

smaller than the total valence number of the four lithium atoms. Thus, super-alkalis as building blocks of electrides can bridge cluster science and solid-state chemistry. Our study demonstrates that using super-alkali, combined with nano-assembly, is a viable strategy for rational design of new electrides with novel properties.

Method

Cluster calculations

The calculations are carried out using the GAUSSIAN 09 package.[29] The hybrid density functional theory (DFT) with Becke three parameter Lee–Yang–Parr (B3LYP)[30,31] functional for exchange–correlation energy and 6-31+G(d,p) basis sets are used. The optimized ground states correspond to stable structures without any imaginary frequency.

Extended structures

Calculations based on Density Functional Theory (DFT) are carried out to optimize the unit cell of the studied materials using Perdew–Burke–Ernzerhof (PBE) generalized gradient approximation (GGA)[32] implemented in the VASP package.[33] The projector augmented wave (PAW)[34] pseudopotential method and a dense Monkhorst–Pack *k*-point mesh are employed in the calculation. The cutoff energy is 550 eV. The energy convergence is set to 10^{-5} eV and the force convergence is set to 0.005 eV Å^{-1}. During the optimization calculations, the van der Waals interaction (as implemented in the DFT+D2 method[35,36]) is considered.

Lattice dynamics

The phonon dispersion relation of the material is calculated using the Density Functional Perturbation Theory (DFPT) including the van der Waals interaction. Geometry of the unit cell is optimized with an energy convergence of 10^{-8} eV and force convergence of 10^{-4} eV Å^{-1}. Phonon frequencies are first calculated on a q-grid of 5 × 5 × 5. Frequencies for other q points are then interpolated from the calculated points.

Molecular dynamics simulations

Ab initio molecular dynamics (AIMD) simulations are conducted using a 1 × 1 × 6 supercell and 1.0 fs time step in an N*V*T ensemble to study the thermodynamics of the materials at room temperature (300 K).

Charge analysis

Bader charge analysis is used to obtain charge distribution on atoms.

Magnetic properties

To find the correct magnetic state of the material, spin polarized optimizations are conducted. The energy of the optimized system is calculated with the tetrahedron method with Blöchl corrections. Very dense *k*-points of (1 × 1 × 21) are sampled in the Brillouin zone to ensure the accuracy.

Conflicts of interest

There are no conflicts to declare.

Acknowledgements

The work is supported in part by the U.S. Department of Energy, Office of Basic Energy Sciences, Division of Materials Sciences and Engineering under Award No. DE-FG02-96ER45579. Resources of the National Energy Research Scientific Computing Center supported by the Office of Science of the U.S. Department of Energy under Contract No. DE-AC02-05CH11231 are also acknowledged. J. Z. acknowledges the Young Talent Support Plan of Xi'an Jiaotong University.

References

1 J. L. Dye, M. R. Yemen, M. G. DaGue and J. Lehn, Optical spectra of alkali metal anion and electride films, *J. Chem. Phys.*, 1978, **68**, 1665.
2 S. Watanabe, T. Watanabe, K. Ito, N. Miyakawa, S. Ito, H. Hosono and S. Mikoshiba, Secondary electron emission and glow discharge properties of $12CaO{\cdot}7Al_2O_3$ electride for fluorescent lamp applications, *Sci. Technol. Adv. Mater.*, 2011, **12**, 034410.
3 H. Yanagi, K. Kim, I. Koizumi, M. Kikuchi, H. Hiramatsu, M. Miyakawa, T. Kamiya, M. Hirano and H. Hosono, Low Threshold Voltage and Carrier Injection Properties of Inverted Organic Light-Emitting Diodes with $[Ca_{24}Al_{28}O_{64}]^{4+}(4e^-)$ Cathode and $Cu_{2-x}Se$ Anode, *J. Phys. Chem. C*, 2009, **113**, 18379.
4 M. Kitano, *et al.* Ammonia Synthesis Using a Stable Electride as an Electron Donor and Reversible Hydrogen Store, *Nat. Chem.*, 2012, **4**, 934.
5 Y. Toda, H. Hirayama, N. Kuganathan, A. Torrisi, P. V. Sushko and H. Hosono, Activation and splitting of carbon dioxide on the surface of an inorganic electride material, *Nat. Commun.*, 2013, **4**, 2378.
6 Y. J. Kim, S. M. Kim, H. Hosono, J. W. Yang and S. W. Kim, The scalable pinacol coupling reaction utilizing the inorganic electride $[Ca_2N]^+{\cdot}e^-$ as an electron donor, *Chem. Commun.*, 2014, **50**, 4791.
7 Y. J. Kim, S. M. Kim, E. J. Cho, H. Hosono, J. W. Yang and S. W. Kim, Two dimensional inorganic electride-promoted electron transfer efficiency in transfer hydrogenation of alkynes and alkenes, *Chem. Sci.*, 2015, **6**, 3577.
8 K. Hayashi, S. Matsuishi, T. Kamiya, M. Hirano and H. Hosono, Light-induced conversion of an insulating refractory oxide into a persistent electronic conductor, *Nature*, 2002, **419**, 462–465.
9 S. Matsuishi, Y. Toda, M. Miyakawa, K. hayashi, T. Kamiya, M. Hirano, I. Tanaka and H. Hosono, High-density electron

anions in a nanoporous single crystal: $[Ca_{24}Al_{28}O_{64}]^{4+}(4e^-)$, *Science*, 2003, **301**, 626–629.
10 Y. Zhang, Z. Xiao, T. Kamiya and H. Hosono, Electron confinement in channel spaces for one-dimensional electride, *J. Phys. Chem. Lett.*, 2015, **6**, 4966–4971.
11 K. Lee, S. W. Kim, Y. Toda, S. Matsuishi and H. Hosono, Dicalcium nitride as a two-dimensional electride with an anionic electron layer, *Nature*, 2013, **494**, 336–340.
12 Y. Zhang, H. Wang, Y. Wang, L. Zhang and Y. Ma, Computer-assisted inverse design of inorganic electrides, *Phys. Rev. X*, 2017, **7**, 011017.
13 T. Inoshita, S. Jeong, N. Hamada and H. Hosono, Exploration for two-dimensional electrides via database screening and ab initio calculation, *Phys. Rev. X*, 2014, **4**, 031023.
14 X. Zhang, Z. Xiao, H. Lie, Y. Toda, S. Matsuishi, T. Kamiya, S. Yeda and H. Hosono, Two-dimensional transition-metal electride Y_2C, *Chem. Mater.*, 2014, **26**, 6638–6643.
15 W. Ming, M. Yoon, M. Du, K. Lee and S. W. Kim, First-principles prediction of thermodynamically stable two-dimensional electrides, *J. Am. Chem. Soc.*, 2016, **138**, 15336–15344.
16 C. Park, S. W. Kim and M. Yoon, First-principle prediction of new electrides with nontrivial and topology based on one-dimensional building blocks, *Phys. Rev. Lett.*, 2018, **120**, 026401.
17 Y. Tsuji, P. L. V. K. Dasari, S. F. Elatresh, R. Hoffmann and N. W. Ashcroft, Structural diversity and electron confinement in Li_4N: potential for 0-D, 2-D, and 3-D electrides, *J. Am. Chem. Soc.*, 2016, **138**, 14108–14120.
18 J. Park, *et al.* Strong localization of anionic electrons at interlayer for electrical and magnetic anisotropy in two-dimensional Y_2C electride, *J. Am. Chem. Soc.*, 2017, **139**, 615–618.
19 S. G. Dale and E. R. Johnson, The explicit examination of the magnetic states of electrides, *Phys. Chem. Chem. Phys.*, 2016, **18**, 27326–27335.
20 T. J. Kim, H. Yoon and M. J. Han, Calculating magnetic interactions in organic elecrides, *Phys. Rev. B*, 2018, **97**, 214431.
21 G. L. Gutsev and A. I. Boldyrev, DVM Xα calculations on the electronic structure of "superalkali" cations, *Chem. Phys. Lett.*, 1982, **92**, 262.
22 T. Zhao, Q. Wang and P. Jena, Rational Design of Superalkalis and Their Roal in CO_2 Activation, *Nanoscale*, 2017, **9**, 4891.
23 H. Fang and P. Jena, Li-Rich Antiperovskite Superionic Conductors based on Cluster Ions, *Proc. Natl. Acad. Sci. U. S. A.*, 2017, **114**, 11046–11051.
24 A. Jain, *et al.* The Materials Project: A materials genome approach to accelerating materials innovation, *APL Mater.*, 2013, **1**(1), 011002.
25 K. Lee, S. W. Kim, Y. Toda, S. Matsuishi and H. Hosono, Dicalcium Nitride as a Two-Dimensional Electride with an Anionic Electron Layer, *Nature*, 2013, **494**, 336.
26 D. P. Wernette, A. S. Ichimura, S. A. Urbin and J. L. Dye, Inorganic Electrides Formed by Alkali Metal Addition to Pure Silica Zeolites, *Chem. Mater.*, 2003, **15**, 1441.
27 H. Freund and M. W. Roberts, *Surf. Sci. Rep.*, 1996, **25**, 225–273.
28 Y. Lu, J. Wang, J. Li, J. Wu, S. Kanno, T. Tada and H. Hosono, Realization of Mott-Insulating Electrides in Dimorphic Yb_5Sb_3, *Phys. Rev. B*, 2018, **98**, 125128.
29 M. J. Frisch, *et al.*, *Gaussian 09, Revision A.02*, Gaussian, Inc., Wallingford, CT, 2016.
30 A. Becke, Density-functional thermochemistry. III. The role of exact exchange, *J. Chem. Phys.*, 1993, **98**, 5648–5652.
31 C. Lee, W. Yang and R. G. Parr, Development of the colle-salvetti correlation-energy formula into a functional of the electron density, *Phys. Rev. B: Condens. Matter Mater. Phys.*, 1998, **37**, 785–788.
32 J. P. Perdew, K. Burke and M. Ernzerhof, Generalized Gradient Approximation Made Simple, *Phys. Rev. Lett.*, 1996, **77**, 3865.
33 G. Kresse and J. Furthmueller, Efficiency of ab-initio total energy calculations for metals and semiconductors using a plane-wave basis set, *J. Comput. Mater. Sci.*, 1996, **6**, 15–50.
34 G. Kresse and J. Furthmueller, Efficient iterative schemes for ab initio total-energy calculations using a plane-wave basis set, *Phys. Rev. B: Condens. Matter Mater. Phys.*, 1996, **54**, 11169–11186.
35 S. Grimme, Semiempirical GGA-type density functional constructed with a long-range dispersion correction, *J. Comput. Chem.*, 2006, **27**, 1787.
36 H. Fang, M. T. Dove and K. Refson, Ag-Ag dispersive interaction and physical properties of $Ag_3Co(CN)_6$, *Phys. Rev. B: Condens. Matter Mater. Phys.*, 2014, **90**, 054302.